Sergio Fragoso, Juan Garrido, Francisco Vázquez, Fernando Morilla, Comparative analysis of decoupling control methodologies and Hinf multivariable robuts control for VS-VP wind turbines, IREC2015 The Sixth International Renewable Energy Congress, Sousse, Tunisia, 2015, pp. 1-6, doi: 10.1109/IREC.2015.7110966. ISBN 978-1-4799-7947-9, IEEE. The version of record of this manuscript has been published and is available at https://ieeexplore.ieee.org/abstract/document/7110966

Comparative analysis of decoupling control methodologies and H_∞ multivariable robust control for VS-VP wind turbines

Sergio Fragoso, Juan Garrido, Francisco Vázquez
Department of Computer Science and Numerical Analysis
University of Cordoba
Córdoba, Spain
p52frhes@uco.es, juan.garrido@uco.es, fvazquez@uco.es

Fernando Morilla
Department of Computer Science and Automatic Control
UNED
Madrid, Spain
fmorilla@dia.uned.es

***Abstract*— Wind turbines systems considered multivariable processes can work in several operational modes. Each mode can be represented with a dynamic model. This fact supposes a difficulty in controlling these types of systems. In addition, the models are subjected undesired interactions between variables. In this paper, different multivariable methodologies are proposed to deal with the previous problems when they are applied to a variable-speed variable-pitch wind turbine. Specifically, the proposed methods to be performed and compared are a multivariable robust control based on the H_∞ mixed sensitivity problem and multivariable control strategies with different decoupling networks.**

Keywords—Wind energy; multivariable control; decoupling networks; robust control.

I. INTRODUCTION

Similar to most industrial processes, the wind turbines are complex and multivariable [1]. These systems involve many variables and most of them have strong interactions. This fact can cause difficulties in feedback controller design. Usually, the generated electric power and the rotor speed are the output variables whereas, the generator torque and blade pitch angle are the manipulated variables.

Wind turbines work in several operational modes. These modes depend on the wind speed as illustrated in Fig. 1.

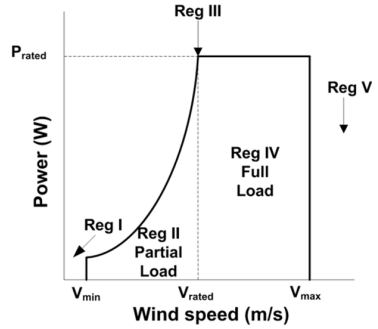

Fig.1. Wind turbine operation modes

In each operational mode, the wind turbine has a dynamic response. This variability in the response means that the system attends to a multi-model process. Being aware of the complexity of this multi-model process, from the control point of view, it could be appropriated to implement a controller which can withstand the coupling and strong uncertainties. According to this, the development of a multivariable robust controller could be adequate. In this paper one in particular is described following the design systematic methodology proposed in [2]: a multivariable H_∞ controller based on the mixed sensitivity problem.

When the wind turbines are addressed as multivariable systems, the problem of coupling or interaction between the control variables is rarely addressed. Traditionally, these kinds of problems have been solved using single-loop PID controllers [3]. This approach is proper when the interaction is moderate [4]. Nevertheless, when the interaction level is more significant, the system performance can be deteriorated. In addition, these interactions particularly occur in the transition zone (Reg. III) between partial load region and full load region. Therefore, in these cases, more complex multivariable control strategies such as decoupling networks can be advisable to reduce the undesired side effects of the single-loop strategies [5]. In this study, also a single decoupling controller is proposed through several decoupling methodologies. The designed decoupling controller pretends to achieve a good performance in all operational modes.

This paper shows a comparative study between two multivariable control methodologies described above: robust control and decoupling networks that address the problem from two different points of view. These methodologies have been compared using as basis the linear model of a lab-scale wind turbine (Fig. 2).

The paper is structured as follows: Section II presents a general description of the lab-scale wind turbine and approximated linear models that are obtained from the identification process. Section III explains the robust control and decoupling networks techniques for multivariable processes, especially for the wind turbine process. In Section IV, simulation results are presented. Finally, the conclusions are summarised in Section V.

II. PROPOSED SYSTEM

This study uses a lab-scale experimental variable-speed variable-pitch (VS-VP) wind turbine for the comparative analysis of the proposed methodologies. This small wind turbine includes a rotor with two blades and direct coupling without a gearbox to a permanent magnet DC electric generator (Fig. 2).

Fig.2. Lab-scale small wind turbine

The general structure of a wind turbine is composed of a mechanical subsystem and an electrical subsystem. The mechanical subsystem consists of the turbine rotor, which includes the aerodynamic components, the gearbox (if any) and the low-speed and high-speed axes. The electrical subsystem is composed of the generator unit, which consists of the electric generator and the static converter that is connected to a load or grid. Shown below summarizes the physical description of these two subsystems in the case of experimental wind turbine.

A. Mechanical subsystem description

Assuming a rigid speed shaft and direct coupling between the rotor and the electric generator, one-mass model can be used to describe the dynamics of this subsystem.

$$J_t \frac{d\omega_r}{dt} = \tau_a - \tau_{em} \tag{1}$$

where ω_r is the rotor speed, τ_{em} is the electromagnetic torque of the generator and τ_a is the aerodynamic torque. J_t is the total inertia moment.

The aerodynamic torque is generated by the wind forces and depends on the aerodynamic properties of the turbine [6]. The torque τ_a is given by the nonlinear expression (2).

$$\tau_a = \frac{1}{2}\rho\pi R^3 \frac{C_p(\lambda,\beta)}{\lambda} v^2 \tag{2}$$

where R is the radius of the rotor, v is the wind speed, λ is the tip-speed ratio (TIP), which is defined as the ratio between the linear blade tip speed and the wind speed.

$$\lambda = \frac{\omega_r R}{v} \tag{3}$$

The power coefficient $C_p(\lambda,\beta)$, which depends on the tip-speed ratio and the blade pitch angle β, is the most important parameter for the design of the control system for the wind turbines, especially in the power regulation case. This coefficient considerably contributes to the non-linear character of the system. In practice, it is difficult to obtain and is different for every wind turbine. However, in this study a polynomial fitting is proposed from the experimental data. By extrapolation techniques, it has been possible to obtain a three-dimensional representation of this power coefficient as a function of the tip-speed ratio and pitch angle. Fig. 3 shows the corresponding surface for the experimental power coefficient of the lab-scale wind turbine.

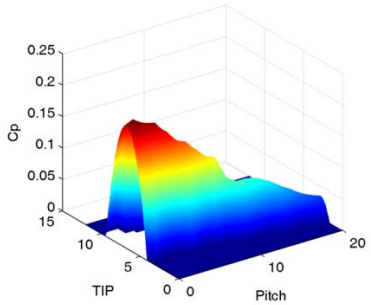

Fig.3. Experimental power coefficient $C_p(\lambda,\beta)$ surface

In the surface shown in Fig. 3, the optimum point is achieved at tip-speed ratio of 6.8 and a pitch angle of 1º.

B. Electrical subsytem description

The lab-scale experimental wind turbine used in this study uses a permanent-magnet DC electric generator. Its field flux is constant, and thus the electromagnetic torque τ_{em} can be modified by controlling the armature current i_g according to (4). Therefore, a change in the generated torque conditions causes a change in the electric power conditions as indicated by equation (5). The parameters η and k_t represent the efficiency and the torque constant of the electric generator, respectively.

$$\tau_{em} = k_t i_g \tag{4}$$

$$P_g = \eta \tau_{em} \omega_r \tag{5}$$

The armature current flows across the load. Modifying this current causes changes in the generated torque and the electric power. This requires having a variable load [7]. The load resistance is modified by activating or deactivating one resistor by pulse-width-modulation (PWM). Using the 2 KHz PWM signal of a generic microcontroller, the apparent resistance can be modified as a function of the duty cycle α between the nominal resistance (100% duty cycle) and free charging circuit (at 0% duty cycle). Hence, increasing the duty cycle decrease the resistance, which produces a larger current i_g to flow through the generator, which increases the generator torque.

C. Linear models

The control techniques proposed in this study are based on linear systems. Therefore, approximate linear models of the real system are necessary to perform the designs. Fig. 4 depicts the proposed general multivariable control scheme.

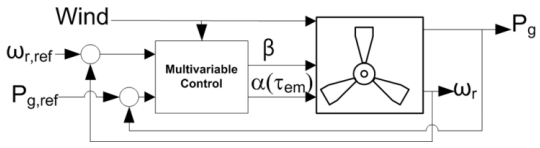

Fig. 4. Multivariable control scheme.

The linear models are obtained by identification and are defined (6), where G(s) is the process transfer matrix, and

$G_D(s)$ is the disturbance matrix associated with the wind speed input.

$$\begin{pmatrix}\omega_r\\ P_g\end{pmatrix} = G(s)\begin{pmatrix}\beta\\ \alpha\end{pmatrix} + G_D(s)v \quad (6)$$

As previously mentioned, the plant has been modelled as multivariable system. The input control vector u is composed of the blade pitch angle β, which ranges from 0º to 25º and the duty cycle α, which ranges from 0% to 100%. The output vector y is composed of the rotational speed ω_r and the generated electric power P_g. From a control point of view, the wind speed v represents a disturbance input for the process.

Several models were obtained at different operational points, which were related with the operational modes of wind turbine: partial load mode, transition mode and full load mode. The identification data were obtained through open loop step tests. For both robust control methodology as decoupling networks methodology, the modelled dynamic in the transition zone with wind speed at 8 m/s was considered as the nominal model for the design process. In this zone, the wind turbine experiences more interaction between variables. This fact is shown in the next epigraph.

The resulting models for each wind speed are shown in Table I.

TABLE I. RESULTING LINEAR MODELS

Wind speed	$G(s)$	$G_D(s)$
6 m/s	$\begin{pmatrix}\frac{-8.059}{75.27s^2+17.35s+1} & \frac{-405.4}{28.25s^2+16.47s+1}\\ \frac{-0.0081479}{16.873s+1} & \frac{4.4195}{1.7589s+1}\end{pmatrix}$	$\begin{pmatrix}\frac{364.9}{118.3s^2+21.76s+1}\\ \frac{1.139}{65.28s^2+17.09s+1}\end{pmatrix}$
7 m/s	$\begin{pmatrix}\frac{-10.534}{97.41s^2+20.63s+1} & \frac{-520.3}{16.61s^2+15.81s+1}\\ \frac{-0.039756}{14.653s+1} & \frac{5.8011}{1.2295s+1}\end{pmatrix}$	$\begin{pmatrix}\frac{340.01}{110.3s^2+21.01s+1}\\ \frac{1.139}{52.72s^2+14.97s+1}\end{pmatrix}$
8 m/s	$\begin{pmatrix}\frac{-8.3951}{118.4s^2+21.77s+1} & \frac{-491.4}{35.36s^2+11.89s+1}\\ \frac{-0.06102}{16.93s+1} & \frac{6.7614}{0.93526s+1}\end{pmatrix}$	$\begin{pmatrix}\frac{345}{104.6s^2+20.45s+1}\\ \frac{2.341}{41.53s^2+14.85s+1}\end{pmatrix}$
9 m/s	$\begin{pmatrix}\frac{-45.251}{113.4s^2+21.37s+1} & \frac{-366.8}{50.86s^2+14.36s+1}\\ \frac{-0.3132}{16.803s+1} & \frac{8.0643}{1.10434s+1}\end{pmatrix}$	$\begin{pmatrix}\frac{287.46}{85.1s^2+18.45s+1}\\ \frac{2.0273}{40.73s^2+12.76s+1}\end{pmatrix}$
10 m/s	$\begin{pmatrix}\frac{-59.06}{116.8s^2+21.62s+1} & \frac{-300.6}{0.01389s^2+13.9s+1}\\ \frac{-0.3932}{16.395s+1} & \frac{8.6291}{1.446s+1}\end{pmatrix}$	$\begin{pmatrix}\frac{248.2}{74.04s^2+17.21s+1}\\ \frac{1.791}{21.91s^2+11.91s+1}\end{pmatrix}$

D. Interaction analysis

The interaction between variables increases the difficulty of controlling a multivariable process. It is important to know the level of interaction to select the suitable control strategy. Table II shows the element λ_{11} of the relative gain array (RGA) for the models shown in Table I. The RGA analysis shows that the experimental wind turbine has a higher level of interaction in the transition operating mode at 8 m/s.

TABLE II. RGA OF THE MODELS

Wind speed	λ_{11} RGA
6 m/s	0.9151
7 m/s	0.7471
8 m/s	0.6543
9 m/s	0.7606
10 m/s	0.8118

III. CONTROLLERS DESIGN

A. The H_∞ mixed sensitivy problem

The multivariable robust controller design problem can be formulated as an H_∞ optimization problem, which responds under the scheme shown in Fig. 5 [2]. In this figure, $P(s)$ is the generalised plant, $K(s)$ is the controller, u are the control signals, ω are the exogenous signals, v the measured variables and z are the error variables.

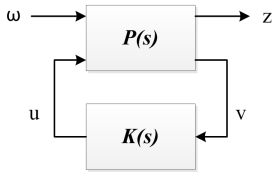

Fig. 5. General formulation of the control problem

B. Robust controller synthesis

The controller synthesis follows the systematic design procedure proposed in [2]. The optimal H_∞ control problem is still no solved, however solutions exists for the suboptimal problem [8]. The control problem with the configuration of Fig. 5 consists of computing a controller such that the ratio γ between the energy of z and the energy of the exogenous signal vector ω is minimised.

A configuration for building up the generalized plant is the *S/KS/T* mixed sensitivity problem [9]. This configuration is shown in Fig. 6 [2]. In this case, the resulting closed loop transfer function $T_{z\omega}(s)$ is expressed as follows:

$$T_{z\omega}(s) = \begin{bmatrix} W_s(s)S_o(s) \\ W_{KS}(s)K(s)S_o(s) \\ W_T(s)T_o(s) \end{bmatrix} \quad (7)$$

where $S_o(s)$ is the output sensitivity transfer matrix, $T_o(s)$ is the output complementary sensitivity transfer matrix, and $K(s)S_o(s)$ is the control sensitivity transfer matrix.

The matrices $W_S(s)$, $W_T(s)$ and $W_{KS}(s)$ are the weighting matrices of the configuration, which allow to specify the range of relevant frequencies for $T_{z\omega}(s)$. The selection of these matrices has been accomplished following design rules.

First step is to obtain the scaled nominal model. This previous process is necessary to estimate the multiplicative output uncertainty for the non-nominal models. The multiplicative output uncertainty affects to the robust stability of the system modifying the shape of $T_o(s)$. A proper shape of output complementary sensitivity transfer matrix is desirable for tracking problems and noise attenuation.

The nominal model can be scaled by means of the following expression:

$$\hat{G}(s) = D_e^{-1}G(s)D_u \quad (8)$$

where $G(s)$ is the original nominal linear model, D_e and D_u are scaling matrices.

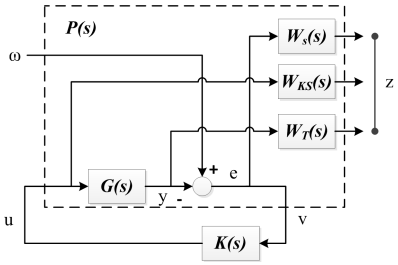

Fig. 6. *S/KS/T* mixed sensitivity configuration

$$D_e = \begin{bmatrix} \Delta\omega_{r\,max} & 0 \\ 0 & \Delta P_{g\,max} \end{bmatrix} = \begin{bmatrix} 436 & 0 \\ 0 & 5.86 \end{bmatrix}$$
$$D_u = \begin{bmatrix} \Delta\beta_{max} & 0 \\ 0 & \Delta\alpha_{max} \end{bmatrix} = \begin{bmatrix} 6 & 0 \\ 0 & 0.55 \end{bmatrix} \quad (9)$$

Once the nominal scaled model is calculated, the multiplicative output uncertainty can be estimated as follows:

$$\hat{E}_{o,i}(s) = \left(\hat{G}_i^*(s) - \hat{G}(s)\right)\hat{G}(s)^{-1}, \quad i = 1,2,\ldots \quad (10)$$

where $\hat{G}_i^*(s)$ represents the different scaled non-nominal systems at each operational points.

Next step it is to design the matrix $W_T(s)$ as a square diagonal matrix with all its diagonal elements with the same transfer function.

$$W_T(s) = W_{Tdiag}(s) \cdot I \quad (11)$$

$W_{Tdiag}(s)$ is a transfer function which must be stable, minimum phase, with high gain at high frequencies, and with magnitude greater than the maximum singular value of the uncertainty computed by the expression (10) for each non-nominal model.

For this study, $W_{Tdiag}(s)$ has been selected as follows:

$$W_{Tdiag}(s) = 0.5623\frac{(50s+1)}{(0.5s+1)} \quad (12)$$

Matrix $W_s(s)$ is obtained as square diagonal matrix of transfer functions:

$$W_s(s) = \begin{bmatrix} W_{s1}(s) & 0 \\ 0 & W_{s2}(s) \end{bmatrix} \quad (13)$$

where each diagonal element $W_{si}(s)$ is described with the expression (14). ω_T is the crossover frequency of $W_{Tdiag}(s)$ and whose value is about 0.0294 rad/s. α_i and β_i are the transfer function gains at high and low frequencies, respectively. According to the design process cited in [2], the following values have been selected: $\alpha_1 = \alpha_2 = 0.5$ and $\beta_1 = \beta_2 = 10^{-4}$. The parameter k_i adjusts the response speed of the outputs. This parameter is chosen heuristically by trial and error method. The following values have been selected: $k_1 = 0.15$ and $k_2 = 1.1$.

$$W_{si}(s) = \frac{\alpha_i s + 10^{(k_i-1)}\omega_T}{s + \beta_i 10^{(k_i-1)}\omega_T}, \qquad i = 1,2 \quad (14)$$

The matrix $W_{KS}(s)$ is chosen as identity matrix to avoid numerical problem in the synthesis algorithm.

Once the weighting matrices have been designed and using computational software, the controller $\widehat{K}(s)$ is synthesised. It is important to remember that the controller calculated has been obtained with the scaled plant, so it is necessary to rebuild this controller by the expression (15).

$$K(s) = D_u\widehat{K}(s)D_e^{-1} \quad (15)$$

The H_∞ synthesis of the controller has a ratio γ equal to 7.95. Considering this fact, and according to (16), this value does not guarantee robust stability, so it is necessary to verify that the sensitivity transfer function and complementary sensitivity transfer functions do not exceed the upper bounded values in the entire range of frequencies [10].

$$\|T_{z\omega}(s)\|_\infty = \left\| \begin{pmatrix} W_s(s)S_o(s) \\ W_{KS}(s)K(s)S_o(s) \\ W_T(s)T_o(s) \end{pmatrix} \right\|_\infty < \gamma \quad (16)$$

Fig. 7 shows the magnitude of maximum singular value of the diagonal elements of $S_o(s)$ and $T_o(s)$, together with the bounded values $W_s^{-1}(s)$ and $W_T^{-1}(s)$.

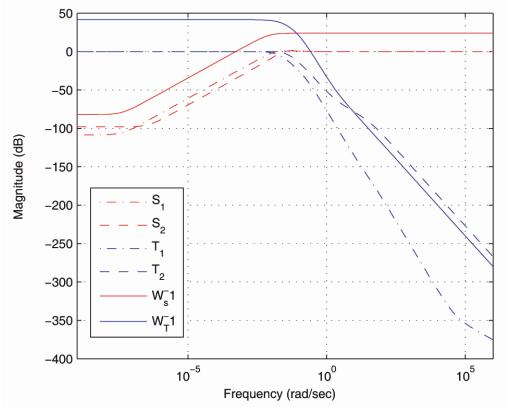

Fig. 7. Diagonal elements of $S_o(s)$ and $T_o(s)$ and the upper bounded values

Generally, the controller $K(s)$ obtained for this procedure is too high order to implement. Considering this fact, the controller should be reduced (e.g., studying the Hankel singular values).

C. Control by decoupling

There are two approaches for centralised control: a pure centralised strategy [11] and a decoupling network that is combined with a diagonal decentralised controller [12]. This paper considers the latter approach.

A decentralised control system with a decoupling network can be designed by combining a diagonal controller $C(s)$ with a block compensator $D(s)$ such that the diagonal controller sees the apparent process $Q(s) = G(s) \cdot D(s)$ as a set of n completely independent processes. Some decoupling schemes are static, and others are dynamic.

Most decoupling approaches use a conventional decoupling scheme in which the process inputs are derived by a time-weighted combination of feedback controller outputs (Fig. 8a).

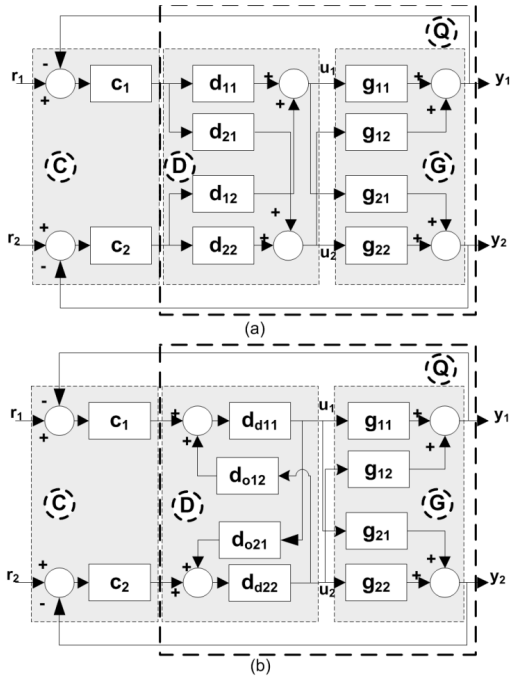

Fig. 8. Decoupling control system of a 2x2 process: (a) conventional decoupling; (b) inverted decoupling [13].

In this study the following three decoupling schemes are used:

- Dynamic simplified decoupling
- Static simplified decoupling
- Inverted decoupling

D. Dynamic simplified decoupling

In dynamic simplified decoupling, n elements of the decoupler, generally the diagonal ones, are set to unity. The general expressions of the decoupler D(s) and the diagonal apparent process Q(s) are cited in [14]. For the nominal model for 8 m/s, the following decoupler is obtained:

$$D(s) = \begin{pmatrix} 1 & \dfrac{-196s^2 - 36.04s - 1.655}{s^2 + 0.34s + 0.028} \\ \dfrac{0.00049s + 0.00053}{s + 0.059} & 1 \end{pmatrix} \quad (17)$$

E. Static simplified decoupling

Static simplified decoupling is a version of simplified decoupling that only decouples the process at the stationary state. The decoupler is only calculated with the information of the stationary gain of the process. Expression (18) shows the static simplified decoupler for the nominal model.

$$D(s) = \begin{pmatrix} 1 & -58.5341 \\ 0.00902 & 1 \end{pmatrix} \quad (18)$$

F. Inverted decoupling

Using the structure of inverted decoupling (Fig. 8b), it is possible to obtain an apparent process in Q(s) that is as simple as the diagonal elements of G(s) while the decoupler elements are the same as those of the dynamic simplified decoupling [13].

In inverted decoupling, the entire decoupler $D(s)$ is divided into two matrices: a diagonal matrix $Dd(s)$ in the direct path and an off-diagonal matrix $Do(s)$ in a feedback path. The expressions of the decoupler matrices and the corresponding apparent process appear in [14]. In this case, the matrix $Dd(s)$ is equal to identity matrix, and $Do(s)$ is given by (19).

$$D_o(s) = \begin{pmatrix} 0 & \dfrac{-289.6s^2 - 61.31s - 2.97}{s^2 + 0.9514s + 0.06017} \\ \dfrac{0.000057505s + 0.000046776}{s + 0.06835} & 0 \end{pmatrix} \quad (19)$$

G. Decentralised controller for decoupling methodologies

The parameters of the diagonal controllers in C(s) can be tuned independently for the corresponding apparent process elements $q_i(s)$ in the methodologies that achieve perfect decoupling, such as dynamic simplified decoupling and inverted decoupling. For these control strategies, the existing SISO PID tuning methods can be directly applied [15]. In the case of non-perfect decoupling methodologies, such as static simplified decoupling, the iterative procedure of [4] was used.

IV. SIMULATION RESULTS

Two simulations are performed using the models shown in Table I and the proposed controllers described in Section III. In particular, the nominal model at 8 m/s and the non-nominal model at 10 m/s are simulated. Fig. 9 and Fig. 10 show the results, respectively. At t=100 s, there is a step change in the reference of P_g, and a step change occurs in the reference of ω_r at t=800 s. The reference step changes are approximately 15% of the outputs at the corresponding operation point.

Numerically, the comparison has been establishes through performance indices such as Integral Absolute Error (IAE) and Standard Deviation (Std) for each control loop. Table III summarizes these performance indices for the two simulations. Above value and below value are the indices for the nominal and non-nominal simulations, respectively.

Table III shows that the robust control generally improves other methodologies in IAE indices whereas that, the decoupling methodologies highlight in the standard deviation.

TABLE III. PERFORMANCE INDICES

	IAE_1	IAE_2	Std_1	Std_2
H_∞	$1.921 \cdot 10^6$ $5.826 \cdot 10^5$	$1.344 \cdot 10^4$ $5.795 \cdot 10^3$	95.68 47.80	0.368 0.202
Simp.	$3.164 \cdot 10^6$ $3.595 \cdot 10^6$	$5.220 \cdot 10^3$ $1.103 \cdot 10^4$	87.91 45.08	0.319 0.118
Stat.	$3.230 \cdot 10^6$ $3.594 \cdot 10^6$	$5.762 \cdot 10^3$ $1.103 \cdot 10^4$	87.58 44.84	0.317 0.121
Inv.	$4.691 \cdot 10^6$ $5.459 \cdot 10^6$	$7.977 \cdot 10^3$ $1.680 \cdot 10^4$	79.82 42.11	0.323 0.126

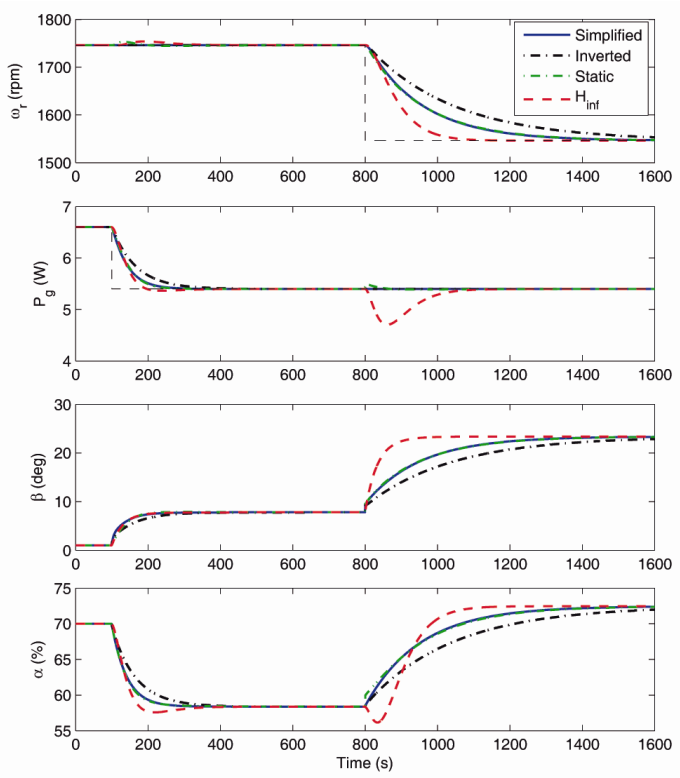

Fig. 9. Outputs and control signals of the simulated closed-loop with the nominal model in the transition mode

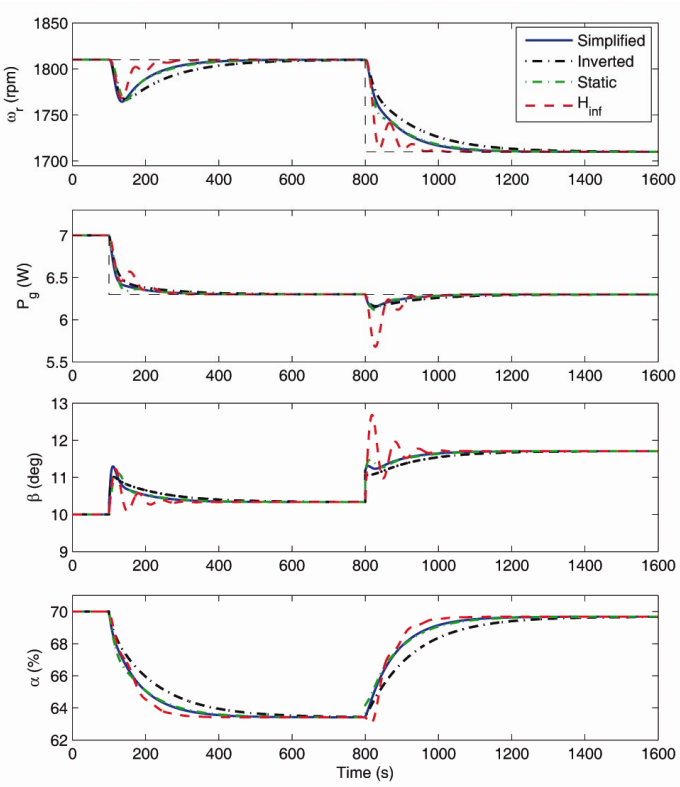

Fig. 10. Outputs and control signal of the simulated closed-loop with the non-nominal model in the full load mode.

V. CONCLUSIONS

This study proposes wind turbines as an example of an industrial multi-model process in which the several dynamics and the interaction between variables can be an important issue for control. These difficulties can be addressed through two control methodologies: robust control, which address the multi-model character, and the decoupling networks, which address the interaction problem.

The simulation results show that both methodologies achieve a good performance for the design nominal point and non-nominal point. Quantitatively, the decoupling methodologies stand out the robust control in the nominal point; however, the latter highlights in the IAE indices for the nominal and non-nominal points. In return, the robust control presents a higher order controller, which is difficult to implement in practice, and it is necessary to reduce.

ACKNOWLEDGMENT

This work was supported by the Autonomous Government of Andalusia (Spain), under the Excellence Project P10-TEP-6056. This support is gratefully acknowledged.

REFERENCES

[1] F. G. Shinskey, *Sistemas de Control de Procesos. Aplicación, Diseño y Sintonización*. New York, New York, USA: McGraw-Hill, 2006.

[2] M. G. Ortega and F. R. Rubio, "Systematic design of weighting matrices for the H∞ mixed sensitivity problem," *J. Process Control*, vol. 14, no. 1, pp. 89–98, Feb. 2004.

[3] L. Y. Pao and K. E. Johnson, "A tutorial on the dynamics and control of wind turbines and wind farms," in *2009 American Control Conference*, 2009, pp. 2076–2089.

[4] F. Vázquez, F. Morilla, and S. Dormido, "An Iterative Method for Tuning Decentralized PID Controllers," in *14th IFAC World Congress*, 1999, pp. 491–496.

[5] J. Garrido, F. Vázquez, F. Morilla, and T. Hagglund, "Practical Advantages of Inverted Decoupling," *Proc. Inst. Mech. Eng. Part I J. Syst. Control Eng.*, vol. 7, pp. 977–992, Jul. 2011.

[6] M. García-Sanz and E. Torres, "Control y Experimentación del Aerogenerador Síncrono de Velocidad Variable TWT1650," *Rev. Iberoam. automática e informática Ind.*, vol. 1, pp. 53–62, 2004.

[7] G. Van Der Veen, "Identification of Wind Energy Systems," Delft Technical University (Holland), 2013.

[8] J. Doyle, K. Glover, P. Khargonekar, and B. Francis, "State-Space Solutions to Standard H2 and Hinf Control Problems," *IEEE Trans. Automat. Contr.*, vol. 34, no. 8, pp. 831–847, 1989.

[9] S. Skogestad and I. Postlethwaite, *Multivariable Feedback Control: Analysis and Design*. John&Wiley, 2005.

[10] A. Alfaya, G. Bejarano, M. G. Ortega, and F. R. Rubio, "Control robusto multivariable de un ciclo de refrigeración," in *XXXV Jornadas de Automática*, 2014, pp. 3–5.

[11] J. Garrido, F. Vázquez, and F. Morilla, "Multivariable PID control by decoupling," *Int. J. Syst. Sci.*, no. October, pp. 1–19, Apr. 2014.

[12] P. Nordfeldt and T. Hagglund, "Decoupler and PID controller design of TITO systems," *J. Process Control*, vol. 16, no. 9, pp. 923–936, 2006.

[13] J. Garrido, F. Vázquez, and F. Morilla, "An Extended Approach of Inverted Decoupling," *J. Process Control*, vol. 21, no. 1, pp. 55–68, Jan. 2011.

[14] F. Morilla, J. Garrido, and F. Vázquez, "Multivariable Control by Decoupling," *Rev. Iberoam. Automática e Informática Ind. RIAI*, vol. 10, no. 1, pp. 3–17, Jan. 2013.

[15] F. Morilla and S. Dormido, "Methodologies for the tuning of PID controllers in the frequency domain," in *Proceedings of PID'00*, 2000, pp. 155–160.